Letter

Competing charge and magnetic order in the candidate centrosymmetric skyrmion host $EuGa_2Al_2$

A. M. Vibhakar,[1,*] D. D. Khalyavin,[2] J. M. Moya,[3,4,5] P. Manuel,[2] F. Orlandi,[2] S. Lei,[4,5] E. Morosan,[3,4,5] and A. Bombardi[1,6]

[1]*Diamond Light Source Ltd, Harwell Science and Innovation Campus, Didcot, Oxfordshire OX11 0DE, United Kingdom*
[2]*ISIS facility, Rutherford Appleton Laboratory-STFC, Chilton, Didcot OX11 0QX, United Kingdom*
[3]*Applied Physics Program, Smalley-Curl Institute, Rice University, Houston, Texas 77005, USA*
[4]*Department of Physics and Astronomy, Rice University, Houston, Texas 77005, USA*
[5]*Rice Center for Quantum Materials (RCQM), Rice University, Houston, Texas 77005, USA*
[6]*Clarendon Laboratory, Department of Physics, University of Oxford, Parks Road, Oxford OX1 3PU, United Kingdom*

(Received 17 April 2023; revised 20 July 2023; accepted 6 September 2023; published 22 September 2023)

$Eu(Ga_{1-x}Al_x)_4$ are centrosymmetric systems that have recently been identified as candidates to stabilize topologically nontrivial magnetic phases, such as skyrmion lattices. In this Letter, we present a high-resolution resonant x-ray and neutron scattering study on $EuGa_2Al_2$ that provides new details of the complex coupling between the electronic ordering phenomena. Our results unambiguously demonstrate that the system orders to form a spin density wave with moments aligned perpendicular to the direction of the propagation vector below 19.5 K, and upon further cooling below 15 K, a cycloid with moments in the *ab* plane, in contrast to what has been reported in the literature. We show that concomitant with the onset of the spin density wave is the suppression of the charge density wave order, indicative of a coupling between the localized $4f$ electrons and itinerant electron density. Furthermore, we demonstrate that the charge density wave order breaks the fourfold symmetry present in the $I4/mmm$ crystal structure, thus declassifying these systems as square-net magnets.

DOI: 10.1103/PhysRevB.108.L100404

The formation of skyrmion lattices (skLs) in materials with centrosymmetric symmetry has prompted an interest in the scientific community to pinpoint the mechanisms stabilizing skyrmion formation in the absence of Dzyaloshinskii-Moriya exchange (DM) interactions [1–7]. The absence of dominant sources of anisotropy and the presence of weakly competing exchange interactions is common to many of the centrosymmetric skyrmion hosts, however the exact mechanism that leads to their formation is not yet understood. Thus far several mechanisms have been proposed, such as geometrical frustration [2,3], Ruderman-Kittel-Kasuya-Yosida (RKKY) interactions mediating a four-spin interaction in itinerant electronic square-net systems [8], and more recently magnetic dipolar interactions [9].

Many centrosymmetric skyrmion hosts are intermetallic, and Gd-based, for instance, $GdPd_2Si_3$ [10,11] $Gd_3Ru_4Al_{12}$ [12], and $GdRu_2Si_2$ [13,14]. More recently, members of the $Eu(Ga_{1-x}Al_x)_4$ series have been identified as candidate skyrmion hosts [15]. For instance, the end member of this series, $EuAl_4$, develops two different skLs under an applied magnetic field [16]. Furthermore, unique to the $Eu(Ga_{1-x}Al_x)_4$ series for $x = 0.5$ and 1 is the development of a charge density wave (CDW) in zero field.

$EuGa_2Al_2$, the focus of this Letter, is electronically and structurally similar to $EuAl_4$ and $GdRu_2Si_2$; it is a rare-earth intermetallic that is expected to mediate magnetic exchange via long range RKKY interactions, the magnetic ions Gd^{3+} and Eu^{2+} are isoelectronic with spin only moments ($L = 0$, $J = 7/2$) [13,16,17]. Furthermore, all three materials have been found to crystallize with $I4/mmm$ symmetry, where the magnetic ions form square nets in the *ab* plane, which are not expected to support any geometrical frustration, and that are coupled along *c* to form a three dimensional network of magnetic ions. The tetragonal symmetry of the crystal structure is thought to allow for the formation of multiple magnetic modulation vectors, which may then develop a double-Q square skyrmion lattice [13]. A topological hall effect analysis of the Hall resistivity in $EuGa_2Al_2$ suggests that a noncoplanar spin texture is stabilized when a magnetic field between $1.2\,T < H < 1.8\,T$ is applied parallel to the *c* axis, and for temperatures below ~ 7 K, hinting at the existence of a topologically nontrivial magnetic phase [15].

Despite its electronic and structural similarity to $EuAl_4$ and $GdRu_2Si_2$, $EuGa_2Al_2$ orders with different magnetic and electronic structures in zero field [16,18,19], indicating it has different underlying electronic interactions. $EuGa_2Al_2$ develops a CDW below $T_{CDW} = 50\,K$, and three magnetic phases below $T_1 = 19.5\,K$, $T_2 = 15\,K$, and $T_3 = 11\,K$, labeled the AFM1, AFM2, and AFM3 phases, respectively [15,17]. Building a theoretical model that can describe the formation

*Corresponding author: anuradha.vibhakar@diamond.ac.uk

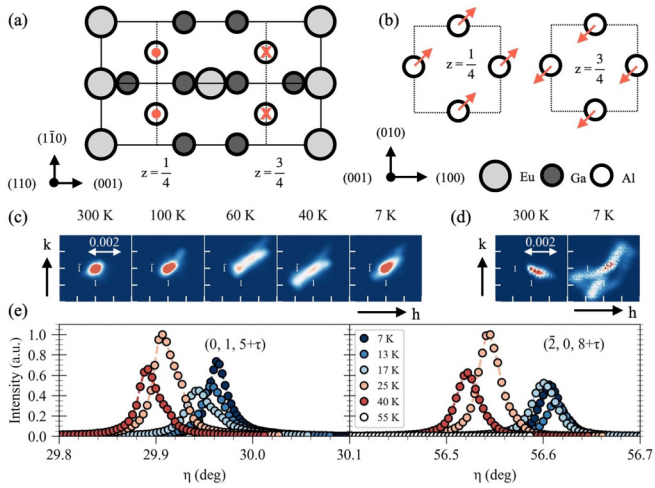

FIG. 1. (a) Single unit cell of $EuGa_2Al_2$ in the $I4/mmm$ space group projected from (110) direction. (b) Cross section of $z = \frac{1}{4}$ and $z = \frac{3}{4}$ planes of the $I4/mmm$ $EuGa_2Al_2$ unit cell projected in the ab plane. $I4/mmm$ unit cell is shown by the solid black line, and the Eu, Ga, and Al ions are given by the gray, black, and white circles, respectively. The red arrows indicate the displacement of the Al ions that would give rise to a charge density wave structure of $Fmmm$ symmetry. Reciprocal space maps of (c) the $(1,\bar{1},8)$ (d) (1,1,8) charge reflections between 300 K and 7 K projected in the hk plane collected at two different positions on the sample. (e) RXS data collected on the $(0,1,5+\tau)$ and $(\bar{2},0,8+\tau)$ CDW reflections between 7 K and 55 K. Data were collected using incident σ polarized light.

of skyrmion lattices in the absence of DM exchange necessitates an accurate experimental determination of the electronic ordering phenomena in such systems and across their phase diagram. To this end, we performed neutron powder diffraction (NPD) and resonant x-ray scattering (RXS) experiments on high-quality single crystals of $EuGa_2Al_2$ that demonstrated the following. First, the onset of the CDW order broke the fourfold symmetry that was present in the $I4/mmm$ crystal structure, and stabilized orthorhombic domains with either $Immm(0, 0, g)s00$) or $Fmmm(0, 0, g)s00$) symmetry. Second, the onset of the magnetic order below T_1 suppressed the CDW order, indicating the two electronic order parameters were in competition. Third, we rigorously demonstrate that $EuGa_2Al_2$ formed a SDW with moments oriented perpendicular to the direction of the propagation vector in the AFM1 phase and a cycloid with moments in the ab plane in the AFM3 phase, in contrast to what has been reported in the literature [15].

In the $I4/mmm$ symmetry the Eu^{2+} ions, Wyckoff position $2a$, form two-dimensional square layers in the ab plane, and neighboring Eu layers, which are separated along c, are translated by $(\frac{1}{2}, \frac{1}{2}, \frac{1}{2})$ owing to the I centering that relates them, as shown in Fig. 1(a). The Al and Ga ions sit between neighboring Eu layers and are ordered across Wyckoff positions $4d$ and $4e$, where Al fully occupies the $4d$ site and Ga the $4e$ site [17], as shown in Fig. 1(b). Single crystals of $EuGa_2Al_2$ were grown in accordance with Refs. [15] and [17]. RXS measurements were performed on the $I16$ beamline at diamond light source [20]. An as grown $1 \times 1 \times 0.5\,mm^3$ single crystal sample was fixed onto a Cu sample holder, and mounted onto a six-circle kappa goniometer. The $(00l)$ was specular, and the $(0k0)$ direction was used as an azimuthal reference. The incident energy was tuned to 6.97 keV, the Eu L_3 edge. Further details of the RXS experiment are given in the Sec. S1 of the Supplemental Material (SM) [21].

At room temperature the crystal was indexed using the published $I4/mmm$ space group [17]. As the sample was cooled a number of distinct changes to the crystal structure were observed. Below 50 K, satellite peaks appeared that were indexed with propagation vector $\mathbf{k} = (0,0,\tau)$, $\tau \sim 0.125$, which were identified to originate in a CDW, consistent with reports in the literature [15]. Owing to the high reciprocal space resolution provided by the $I16$ beamline, it was possible to observe for the first time subtle changes to the crystal structure as we cooled through the CDW and magnetic phase transitions. We observed an elongation of the structural Bragg reflections in the hk plane below T_{CDW}, indicating a loss to the fourfold symmetry that was present at 300 K. The possible subgroups of the displacive representation of the incommensurate CDW propagation vector, $\mathbf{k} = (0,0,\tau)$, consistent with a loss to the fourfold symmetry, are the orthorhombic space groups $Immm(0, 0, g)s00$ and $Fmmm(0, 0, g)s00$. Each of the two orthorhombic subgroups would produce a distinct splitting of $(1,1,l)$ type reflections, as illustrated in Sec. S2 of the SM. For instance, Fig. 1(c) shows the $(1,\bar{1},8)$, which begins to split close to the (1,1,0) direction as the temperature approaches T_{CDW}, consistent with the presence of domains of $Immm(0, 0, g)s00$ symmetry. Upon moving to different positions on the sample, Fig. 1(d), we observed a splitting of the (1,1,8) that was consistent with the presence of domains of $Fmmm(0, 0, g)s00$ symmetry instead, see Sec. S2 of the SM for further details. Whether this points to phase coexistence or an effect of local strains is not clear at present. Nevertheless, this finding demonstrates that $EuGa_2Al_2$ is not a square-net magnet, similar to $EuAl_4$ [24].

Systematic searches along high symmetry lines and points in reciprocal space were made to identify the propagation vector of the magnetic ordering at temperatures representative of the three magnetically ordered phases. The origin of new intensity was investigated by measuring its polarization, azimuthal, and temperature dependence. Magnetic intensity was identified if, at resonance, the intensity was present in either the $\sigma\pi$, $\pi\sigma$, or $\pi\pi$ channels, and absent in the $\sigma\sigma$ channel, Sec. S4 of the SM, and if temperature dependent changes to the intensity were consistent with the magnetic susceptibility data presented in Ref. [17].

Below T_1 we measured several magnetic reflections that indexed with propagation vector, $\mathbf{k} = (\alpha,0,0)$ or $\mathbf{k} = (0,\beta,0)$, where α and β varied between 0.196 and 0.188 according to the temperature, Fig. 2. Sudden changes to these satellite reflections appeared at T_1, T_2, and T_3, Fig. 2(a), confirming the presence of the magnetically ordered phases previously reported [15]. The α and β satellites were observed at a position in the sample representative of a single orthorhombic domain, demonstrating that the orthorhombic domain was further split into two magnetic domains. This pattern of magnetic domains is consistent with $Fmmm(0, 0, g)s00$ symmetry of the orthorhombic paramagnetic structure. In the case of $Immm(0, 0, g)s00$ symmetry, only one magnetic satellite (either α or β) should be expected for a single orthorhombic domain. Even though the observation of the two magnetic

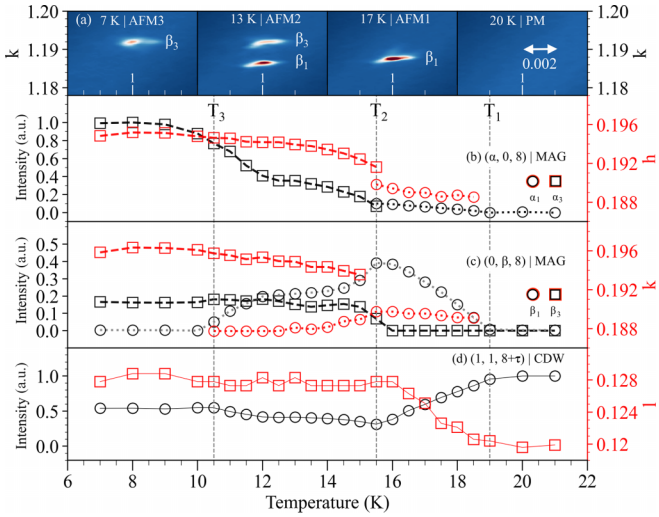

FIG. 2. (a) Reciprocal space maps centered about the $(1,1+\beta,8)$ reflection in the hk plane collected in the PM, AFM1, AFM2, and AFM3 phases. Temperature dependence of the normalized integrated intensity and the magnitude of the propagation vector of (b) $(\alpha,0,8)$, (c) $(0,\beta,8)$, and (d) $(1,1,8+\tau)$ reflections. We note that α_1 and β_1 refer to the magnetic satellites found exclusively in the AFM1 phase, and α_3 and β_3 refer to the magnetic satellites found exclusively in the AFM3 phase. These data were collected using incident σ polarized light.

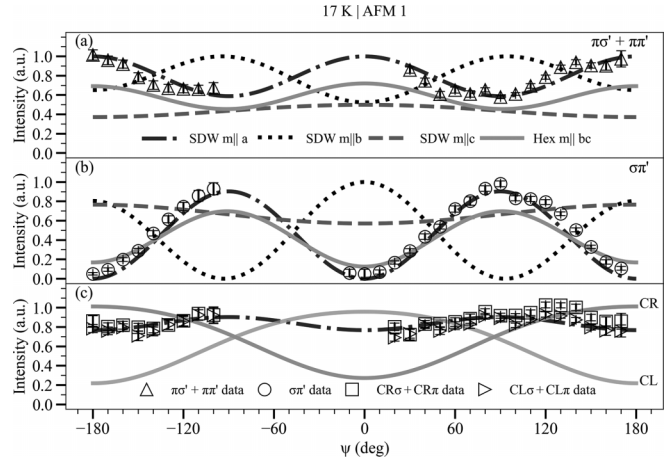

FIG. 3. Scattered intensity plotted as a function of azimuth collected in (a) $\pi\sigma' + \pi\pi'$ channels, (b) $\sigma\pi'$ channel, and (c) the CRσ + CRπ and CLσ + CLπ channels for the $(0,\beta,8)$ reflection at 17 K, in the AFM1 phase. Unfilled markers represent the normalized data. Lines represent the simulated azimuthal dependencies for the different magnetic structure solutions. Details of the simulations are presented in Sec. S4 of the SM.

domains strongly suggests the F-centered cell, we cannot exclude the presence of some fraction of $Immm(0,0,g)s00$ phase, too, as follows from splitting of the fundamental reflections discussed above. An alternative explanation for the presence of both α and β satellites is a two-k magnetic order, which onsets on top of the F-centred orthorhombic structure. In this scenario, however, one should expect the presence of structural distortions with $(\alpha,\beta,0)$ propagation vector. No such satellites were found experimentally. No intensity was observed at reflections where $h+k+l=2n+1, n \in Z$, nor α and β magnetic satellites centered about them, implying the I centring relating the Eu1 and Eu2 ions was not broken in the three magnetic phases, as shown in Fig. S6 of the SM [21].

We describe the temperature dependent changes observed for the $(\alpha,0,8)$ and $(0,\beta,8)$ magnetic satellites belonging to a single orthorhombic domain measured upon warming. For the $(\alpha,0,8)$ reflection, a single peak, labeled α_3, was observed in the AFM3 phase, Fig. 2(b). The intensity of this peak decreased to zero as the system was warmed to the AFM1 phase. At T_2, a second peak labeled α_1 appeared, such that the α_1 and α_3 peaks coexisted over a temperature interval of 0.5 K. The intensity of the α_1 peak was maximized at T_2 before steadily decreasing to zero as the system was warmed to the paramagnetic (PM) phase. A similar dependence was observed for $(0,\beta,8)$, Fig. 2(c), with the exception that the coexistence of the β_1 and β_3 peaks occurred over a wider temperature interval of 4 K. This suggests that the two peaks α_1/β_1 and α_3/β_3 are representative of the AFM1 and AFM3 phases, respectively, and originate in two competing magnetic phases. Note that the difference in the coexistence region of the two magnetic domains can depend on microscopic characteristics such as their size.

The evolution of the propagation vector and intensity of the $(1,1,8+\tau)$ CDW reflection was followed through the magnetic phase transitions to establish the coupling between these phenomena. The intensity of the CDW almost halved, while the value of τ steadily increased between T_1 and T_2, as shown in Fig. 2(d). The temperature dependence of thirty different CDW reflections were subsequently collected as the crystal was warmed through the magnetically ordered phases, as shown in Fig. S4 of the SM [21], which all showed a significant decrease to the intensity of the CDW reflections at the onset of the magnetic order, demonstrating that the CDW was in competition with the magnetic order.

The electrons that give rise to the CDW are itinerant and expected to originate from Al ions [25], while the electrons responsible for the magnetic order are the localized $4f$ electrons on the Eu sites. If the onset of the magnetic order polarizes the itinerant electronic density that gives rise to the CDW, it is feasible that that it could destabilize the CDW order and thus cause its suppression. Indeed, theoretically it has been shown that the spin of the conduction electrons tends to align with the underlying local moment texture in such itinerant magnets [4]. Another mechanism of cross coupling between the SDW and CDW involves totally symmetric tetragonal strain. Both distortions couple the strain implying that onset of the magnetic order renormalizes the CDW through the magnetoelastic coupling. A similar mechanism is particularly relevant for some intermetallic systems [26], where the structural distortion selects the magnetic propagation vector and locks it into commensurate ratio with the periodicity of the CDW. Below T_2 we also observed a change to the relative intensity of different CDW reflections, Fig. 1(e), which indicates that the structure of the CDW was changing. We note that for $EuAl_4$, a CDW with orthorhombic symmetry with a similar propagation vector, $\mathbf{k}=(0,0,0.1781(3))$ was observed, where the CDW order was not thought to originate in a simple nesting of the Fermi surface [24,25].

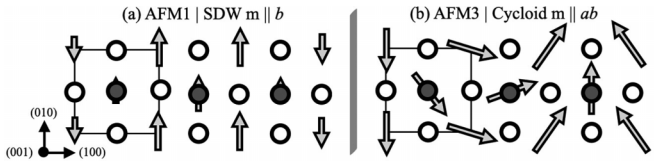

FIG. 4. (a) Representation of the experimentally determined AFM1 and AFM3 magnetic structures projected in the *ab* plane for $(0.5 \leqslant z \leqslant 1)$. Gray arrows represent the moments on the Eu ions, and the Ga and Al ions are denoted by the dark gray and white circles, respectively. The $I4/mmm$ crystallographic unit cell is shown by the solid black line. Moments on Eu ions separated along c are coupled ferromagnetically.

Using magnetic symmetry analysis we identified nine different magnetic structures that the system could adopt, shown in Sec. S3 of the SM. The magnetic structures differ according to the moment direction adopted by the Eu ions, and also according to whether they are collinear (SDW) or noncollinear (helix and cycloid). The resonant magnetic x-ray scattering (RMXS) cross section for the $\sigma\pi'$ channel is dependent on the dot product between the incident wave vector, $\hat{k}_i$, and the magnetic interaction vector, which enables us to determine the direction of the magnetic moments on the Eu ions in the crystal by rotating the crystal relative to the magnetic interaction vector, keeping the incident beam fixed, and measuring the variation in the scattered signal. This is known as an azimuthal scan.

Figure 3 shows the azimuthal scan collected on the $(0,\beta,8)$ in the $\sigma\pi'$ channel at 17 K in the AFM1 phase. Maximums in the intensity of the scattered signal were measured at $\psi = 90^\circ$ and $\psi = -90^\circ$, when $\hat{k}_i$ was parallel to the a axis, therefore a component of the magnetic moment was oriented along a. Furthermore, as the diffracted intensity was zero at ψ of 0, 180°, and -180°, the b- or c-axis component to the magnetic moment was not present. Measurements with incident circular light can be used to determine if the magnetic structure is noncollinear, as explained in Sec. S4 of the SM. The difference in the scattered intensity between the CR and CL light was zero across the majority of azimuthal values measured, Fig. 3(c), indicating the AFM1 phase was collinear. The best fit to the azimuthal dependencies collected on the $(\pm\alpha,0,8)$ and $(0,\pm\beta,8)$ reflections measured with all four incident polarization of light, details of which are given in Sec. S4 of the SM and shown for the $(0,\beta,8)$ in Fig. 3, was a SDW with moments aligned perpendicular to the direction of the propagation vector, consistent with the observations above. This magnetic structure solution, shown in Fig. 4(a), transforms by a single irrep, which is consistent with the PM to AFM1 phase transition being second order in nature. The adoption of the moments perpendicular to the direction of the propagation vector is similar to that observed for $EuAl_4$ [27] and Gd_2PdSi_3 [9], suggesting an anisotropy term that may be common to many of the centrosymmetric skyrmion hosts.

Below 11 K, in the AFM3 phase, $EuAl_4$ develops a noncollinear magnetic structure, owing to the observation of a difference in the scattered intensity when measured using the two incident circular polarizations of light, as shown for the $(0,\beta,8)$ in the inset of Fig. 5(a). A determination of moment direction using an azimuthal scan was not possible,

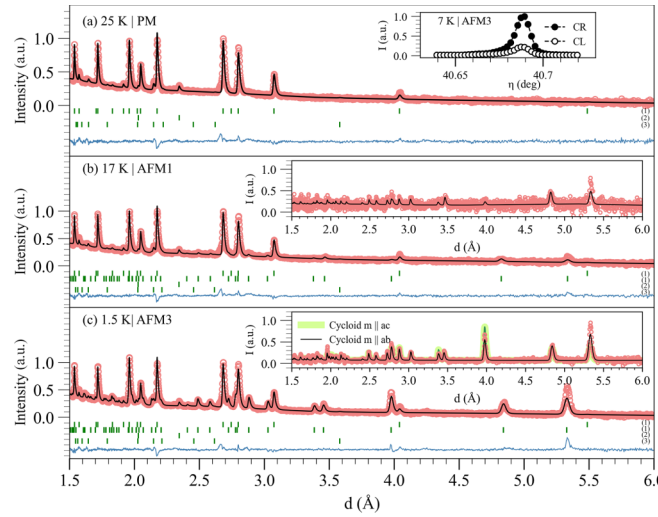

FIG. 5. NPD data collected on WISH at ISIS on $EuGa_2Al_2$ at temperatures (a) 25 K, (b) 17 K, and (c) 1.5 K. Inset in (a) shows the RMXS data collected on $(0,\beta,8)$ magnetic satellite with CR and CL incident light. Insets in (b) and (c) show the subtracted NPD data (25 K data was subtracted) giving only the magnetic reflections. The fit to the data was made with a SDW m||b at 17 K and a circular cycloid with moments in the *ab* plane at 1.5 K. The data is given by the red circles, the fit of the data by the solid black line, and their difference as a blue line. The green tick marks are the nuclear and magnetic reflections from top to bottom of $EuGa_2Al_2$, labeled (1), and the impurity phases, labeled (2) and (3).

owing to the appearance of additional peaks that changed significantly with sample position, and hence, azimuth. Given that a noncollinear magnetic structure would split each magnetic domain into a further two magnetic domains related by inversion symmetry, the appearance of the additional peaks was likely owing to the complex domain structure.

NPD can average over multiple magnetic domains, thereby enabling one to determine the magnetic structure without prior knowledge of the domain structure. Therefore, we used NPD to determine the ground state magnetic ordering in the AFM3 phase. Several single crystal samples of $EuGa_2Al_2$ produced from the same growth were finely crushed to produce a 0.95 g polycrystalline sample, which was measured using the time-of-flight neutron diffractometer WISH at ISIS [28], at 25 K, 17 K, 13 K, and 1.5 K representative of the paramagnetic, AFM1, AFM2, and AFM3 phases, respectively. The orthorhombic distortion measured using RXMS was not observed in the NPD data, owing to the coarser resolution provided by neutron diffraction, and thus, in the PM phase the data were fit using the published $I4/mmm$ crystal structure as shown in Fig. 5(a), and a good fit was achieved, $R = 2.59\%$, $wR = 3.39\%$, $R_{\text{Bragg}} = 15.0\%$.

The magnetic structure could not be determined from the NPD data collected in the AFM1 phase, shown in Fig. 5(b), owing to the appearance of weak magnetic intensity despite long counting times. This is likely due to a small moment developing on the Eu site, coupled with the large Eu neutron absorption cross section. Similarly, a magnetic structure determination from the NPD data collected in the AFM2 phase was not possible as the resolution was not sufficient to distinguish

between the two peaks that appeared in this phase observed using RXMS, as shown in Fig. S9 of the SM [21]. Each of the nine magnetic structure models presented in Sec. S3 were used to refine the NPD collected at 1.5 K. The best fit to the data was a cycloidal magnetic structure model with moments orientated in the *ab* plane. The data were fit using a circular cycloid, shown in Fig. 4(b), as insufficient counting statistics were collected to be able to determine the ellipticity. An excellent fit to the data was achieved, $R = 2.65\%$, $wR = 3.39\%$, $R_{\mathrm{Mag}} = 16.6\%$, as shown in Fig. 5(c). We note that the high value of R_{Bragg} and R_{Mag} is owing to the large Eu neutron absorption cross section. Further details of the Rietveld refinements are given in Sec. S5 of the SM.

The sudden changes to the propagation vector and intensity of the magnetic satellites at T_2, shown in Fig. 2, is consistent with this phase transition being first order in nature. A region of phase coexistence is common following a first order phase transition, and taken together with the observation of the AFM1 and AFM3 peaks coexisting in the AFM2 phase, Fig. 2(a), we question whether there are three distinct magnetically ordered phases. We suggest that the signature of the phase transition in the specific heat capacity at T_3 reported in Ref. [17] may be related to the onset of a structural phase transition as indicated by small changes to the relative intensity of the CDW reflections observed between T_2 and T_3, Fig. 1, consistent with the structure of the CDW changing. While the change to the magnetic susceptibility at T_3, Ref. [17], may be related to a shift in the magnetic domain pattern caused by a complete suppression of the AFM1 phase and the creation of inversion domains.

We propose that if the CDW structure does transform below T_2 it may cause a change to the itinerant electronic density, which in turn may modify the RKKY interactions, resulting in the sudden jump of the propagation vector, Fig. 2. The sequence of the magnetic phases from high temperature SDW to constant moment ground state has been observed in many systems with competing exchange interactions [29,30]. In the AFM1 phase, the partially ordered state is favored by entropy and the moment direction is dictated by anisotropic interactions. In the ground state, the ordered patterns with fully saturated moments are preferred in systems where the magnetic moment is associated with localized electrons. Although Eu^{2+} is a nominally isotropic cation, the weak magnetic anisotropy in $EuGa_2Al_2$ might originate from magnetoelastic coupling, which serves to optimize exchange interactions through structural distortions controlled by the symmetry of the magnetically ordered state. The moment direction adopted in the SDW and ground state are defined by the magnetic symmetry of the system, where the appropriate structural distortions are selected to optimize the elastic and exchange energy.

In conclusion, our study of $EuGa_2Al_2$ has shown that the onset of the CDW order breaks the fourfold symmetry present in the $I4/mmm$ crystal structure stabilizing orthorhombic domains, which demonstrates $EuGa_2Al_2$ is not a square-net magnet. We find that the single crystal samples of $EuGa_2Al_2$ are composed of magnetic domains described by propagation vector $(\alpha,0,0)$ or $(0,\beta,0)$, which order in the AFM1 phase by a SDW with moments perpendicular to the direction of the propagation vector. We observed a suppression of the CDW order as the system ordered to form the SDW, suggesting the two electronic ordering phenomena were in competition, which in turn implies that the localized $4f$ electrons and itinerant electronic density are coupled. Finally, our results show that the ground state magnetic structure was a cycloid with moments in the *ab* plane. Our findings map the zero-field magnetic and structural phases of $EuGa_2Al_2$, revealing more complexity than was previously discovered, and demonstrating the requirement for high-resolution scattering studies to elucidate the true nature of the complex ordering present in such candidate centrosymmetric skyrmion hosts.

We acknowledge Diamond Light Source for time on beamline I16 under Proposals No. MM30799-1 and No. MM34149-1. We gratefully acknowledge the Science and Technology Facilities Council (STFC) for access to neutron beamtime at the WISH diffractometer at ISIS [31]. D.D.K. acknowledges EPSRC support under Grant No. EP/W00562X/1. J.M.M., S.L., and E.M. acknowledge partial support from NSF DMR Grant No. 1903741 and the Robert A. Welch Foundation Grant No. C-2114.

[1] S. Ishiwata, T. Nakajima, J.-H. Kim, D. S. Inosov, N. Kanazawa, J. S. White, J. L. Gavilano, R. Georgii, K. M. Seemann, G. Brandl, P. Manuel, D. D. Khalyavin, S. Seki, Y. Tokunaga, M. Kinoshita, Y. W. Long, Y. Kaneko, Y. Taguchi, T. Arima, B. Keimer *et al.*, Phys. Rev. B **101**, 134406 (2020).

[2] T. Okubo, S. Chung, and H. Kawamura, Phys. Rev. Lett. **108**, 017206 (2012).

[3] A. O. Leonov and M. Mostovoy, Nat. Commun. **6**, 8275 (2015).

[4] C. D. Batista, S.-Z. Lin, S. Hayami, and Y. Kamiya, Rep. Prog. Phys. **79**, 084504 (2016).

[5] S.-Z. Lin and S. Hayami, Phys. Rev. B **93**, 064430 (2016).

[6] R. Ozawa, S. Hayami, and Y. Motome, Phys. Rev. Lett. **118**, 147205 (2017).

[7] R. Yambe and S. Hayami, Sci. Rep. **11** 11184 (2021).

[8] S. Hayami and Y. Motome, Phys. Rev. B **103**, 024439 (2021).

[9] J. A. M. Paddison, B. K. Rai, A. F. May, S. Calder, M. B. Stone, M. D. Frontzek, and A. D. Christianson, Phys. Rev. Lett. **129**, 137202 (2022).

[10] T. Kurumaji, T. Nakajima, M. Hirschberger, A. Kikkawa, Y. Yamasaki, H. Sagayama, H. Nakao, Y. Taguchi, T. hisa Arima, and Y. Tokura, Science **365**, 914 (2019).

[11] M. Hirschberger, L. Spitz, T. Nomoto, T. Kurumaji, S. Gao, J. Masell, T. Nakajima, A. Kikkawa, Y. Yamasaki, H. Sagayama *et al.*, Phys. Rev. Lett. **125**, 076602 (2020).

[12] M. Hirschberger, T. Nakajima, S. Gao, L. Peng, A. Kikkawa, T. Kurumaji, M. Kriener, Y. Yamasaki, H. Sagayama, H. Nakao *et al.*, Nat. Commun. **10**, 5831 (2019).

[13] N. D. Khanh, T. Nakajima, X. Yu, S. Gao, K. Shibata, M. Hirschberger, Y. Yamasaki, H. Sagayama, H. Nakao, L. Peng *et al.*, Nat. Nanotechnol. **15**, 444 (2020).

[14] Y. Yasui, C. J. Butler, N. D. Khanh, S. Hayami, T. Nomoto, T. Hanaguri, Y. Motome, R. Arita, T.-h. Arima, Y. Tokura *et al.*, Nat. Commun. **11**, 5925 (2020).

[15] J. M. Moya, S. Lei, E. M. Clements, C. S. Kengle, S. Sun, K. Allen, Q. Li, Y. Y. Peng, A. A. Husain, M. Mitrano, M. J. Krogstad, R. Osborn, A. B. Puthirath, S. Chi, L. Debeer-Schmitt, J. Gaudet, P. Abbamonte, J. W. Lynn, and E. Morosan, Phys. Rev. Mater. **6**, 074201 (2022).

[16] R. Takagi, N. Matsuyama, V. Ukleev, L. Yu, J. S. White, S. Francoual, J. R. Mardegan, S. Hayami, H. Saito, K. Kaneko *et al.*, Nat. Commun. **13**, 1472 (2022).

[17] M. Stavinoha, J. A. Cooley, S. G. Minasian, T. M. McQueen, S. M. Kauzlarich, C.-L. Huang, and E. Morosan, Phys. Rev. B **97**, 195146 (2018).

[18] Private Communication.

[19] K. Kaneko, T. Kawasaki, A. Nakamura, K. Munakata, A. Nakao, T. Hanashima, R. Kiyanagi, T. Ohhara, M. Hedo, T. Nakama, and Y. Ōnuki, J. Phys. Soc. Jpn. **90**, 064704 (2021).

[20] S. P. Collins, A. Bombardi, A. R. Marshall, J. H. Williams, G. Barlow, A. G. Day, M. R. Pearson, R. J. Woolliscroft, R. D. Walton, G. Beutier, and G. Nisbet, AIP Conf. Proc. **1234**, 303 (2010).

[21] See Supplemental Material at https://link.aps.org/supplemental/10.1103/PhysRevB.108.L100404 for further details of the resonant x-ray scattering experiments, the analysis used to determine the symmetry of the incommensurately modulated crystal structure, temperature dependent data of the charge density wave reflections, the magnetic symmetry analysis, details of the resonant magnetic x-ray simulations, data used to determine the magnetic structure in the AFM1 phase, and the refinement of the neutron powder diffraction data used to determine the magnetic structure in the AFM3 phase. It also contains Refs. [22,23].

[22] S. Watanabe, A. K. Adya, L. Rycerz, A. C. Barnes, M. Gaune-Escard, Y. Okamoto, H. Akatsuka, and H. Matsuura, Prog. Nucl. Energy **47**, 632 (2005).

[23] B. J. Campbell, H. T. Stokes, D. E. Tanner, and D. M. Hatch, J. Appl. Crystallogr. **39**, 607 (2006).

[24] S. Ramakrishnan, S. R. Kotla, T. Rekis, J.-K. Bao, C. Eisele, L. Noohinejad, M. Tolkiehn, C. Paulmann, B. Singh, R. Verma, B. Bag, R. Kulkarni, A. Thamizhavel, B. Singh, S. Ramakrishnan, and S. van Smaalen, IUCrJ **9**, 378 (2022).

[25] M. Kobata, S.-i. Fujimori, Y. Takeda, T. Okane, Y. Saitoh, K. Kobayashi, H. Yamagami, A. Nakamura, M. Hedo, T. Nakama, and Y. Ōnuki, J. Phys. Soc. Jpn. **85**, 094703 (2016).

[26] T. H. Salters, F. Orlandi, T. Berry, J. F. Khoury, E. Whittaker, P. Manuel, and L. M. Schoop, Phys. Rev. Mater. **7**, 044203 (2023).

[27] Private Communication.

[28] L. C. Chapon, P. Manuel, P. G. Radaelli, C. Benson, L. Perrott, S. Ansell, N. J. Rhodes, D. Raspino, D. Duxbury, E. Spill, and J. Norris, Neutron News **22**, 22 (2011).

[29] M. Kenzelmann, A. B. Harris, S. Jonas, C. Broholm, J. Schefer, S. B. Kim, C. L. Zhang, S.-W. Cheong, O. P. Vajk, and J. W. Lynn, Phys. Rev. Lett. **95**, 087206 (2005).

[30] A. Daoud-Aladine, B. Kundys, C. Martin, P. G. Radaelli, P. J. Brown, C. Simon, and L. C. Chapon, Phys. Rev. B **80**, 220402(R) (2009).

[31] A. M. Vibhakar, D. D. Khalyavin, J. M. Moya, P. Manuel, F. Orlandi, S. Lei, E. Morosan, and A. Bombardi, doi:10.5286/ISIS.E.RB2310461.